PLOS ONE

RESEARCH ARTICLE

Designing peptides predicted to bind to the omicron variant better than ACE2 via computational protein design and molecular dynamics

Thassanai Sitthiyotha, Wantanee Treewattanawong, Surasak Chunsrivirot*

Structural and Computational Biology Research Unit, Department of Biochemistry, Faculty of Science, Chulalongkorn University, Pathumwan, Bangkok, Thailand

* surasak.ch@chula.ac.th

Check for updates

OPEN ACCESS

Citation: Sitthiyotha T, Treewattanawong W, Chunsrivirot S (2023) Designing peptides predicted to bind to the omicron variant better than ACE2 via computational protein design and molecular dynamics. PLoS ONE 18(10): e0292589. https://doi.org/10.1371/journal.pone.0292589

Editor: Syed Hani Abidi, Nazarbayev University School of Medicine, PAKISTAN

Received: April 25, 2023

Accepted: September 25, 2023

Published: October 10, 2023

Copyright: © 2023 Sitthiyotha et al. This is an open access article distributed under the terms of the Creative Commons Attribution License, which permits unrestricted use, distribution, and reproduction in any medium, provided the original author and source are credited.

Data Availability Statement: All relevant data are within the paper and its Supporting Information files.

Funding: This study was funded by the Structural and Computational Biology Research Unit, Department of Biochemistry, Faculty of Science, Rachadaphiseksomphot Endowment Fund, Chulalongkorn University, Thailand. The funders had no role in study design, data collection and analysis, decision to publish, or preparation of the manuscript.

Abstract

Brought about by severe acute respiratory syndrome coronavirus 2 (SARS-CoV-2), coronavirus disease (COVID-19) pandemic has resulted in large numbers of worldwide deaths and cases. Several SARS-CoV-2 variants have evolved, and Omicron (B.1.1.529) was one of the important variants of concern. It gets inside human cells by using its S1 subunit's receptor-binding domain (SARS-CoV-2-RBD) to bind to Angiotensin-converting enzyme 2 receptor's peptidase domain (ACE2-PD). Using peptides to inhibit binding interactions (BIs) between ACE2-PD and SARS-CoV-2-RBD is one of promising COVID-19 therapies. Employing computational protein design (CPD) as well as molecular dynamics (MD), this study used ACE2-PD's α1 helix to generate novel 25-mer peptide binders (SPB25) of Omicron RBD that have predicted binding affinities ($\Delta G_{bind\ (MM\text{-}GBSA)}$) better than ACE2 by increasing favorable BIs between SPB25 and the conserved residues of RBD. Results from MD and the MM-GBSA method identified two best designed peptides ($SPB25_{T7L/K11A}$ and $SPB25_{T7L/K11L}$ with $\Delta G_{bind\ (MM\text{-}GBSA)}$ of −92.4 ± 0.4 and −95.7 ± 0.5 kcal/mol, respectively) that have better $\Delta G_{bind\ (MM\text{-}GBSA)}$ to Omicron RBD than ACE2 (−87.9 ± 0.5 kcal/mol) and SPB25 (−71.6 ± 0.5 kcal/mol). Additionally, they were predicted to have slightly higher stabilities, based on their percent helicities in water, than SBP1 (the experimentally proven inhibitor of SARS-CoV-2-RBD). Our two best designed SPB25s are promising candidates as omicron variant inhibitors.

Introduction

The coronavirus disease 2019 (COVID-19) pandemic was caused by severe acute respiratory syndrome coronavirus 2 (SARS-CoV-2) and brought about substantial worldwide cases and deaths [1, 2]. This virus has evolved its genome over time, and several variants of concern such as Alpha (B.1.1.7), Beta (B.1.351), Gamma (P.1), Delta (B.1.617.2), and Omicron (B.1.1.529) variants have emerged [3]. Some mutations may modify viral properties, transmissibility, and

Competing interests: The authors have declared that no competing interests exist.

therapeutic solutions including the performance of vaccines [4]. Structurally, this virus has four principal components such as the spike (S) proteins, envelope (E), nucleocapsid (N) and membrane (M) [5, 6]. The receptor binding (S1) as well as membrane fusion (S2) subunits are in the spike protein. To attach to human cells, this virus uses its S1 subunit's receptor binding domain (RBD) to bind to angiotensin-converting enzyme 2 (ACE2) receptor's peptidase domain (PD) in human, while it uses its S2 subunit for the membrane fusion between its membrane and a host membrane [7, 8]. The previous study found that RBDs of Omicron and SARS-CoV-2 bound to monomeric human ACE2 receptor with the dissociation constant (K_D) of 38.9 ± 10.5 nM and 75.5 ± 2.1 nM, respectively [9].

To inhibit the virus from entering human cells, blocking binding interactions (BIs) between ACE2-PD and RBD using peptide inhibitors, neutralizing antibodies and small-molecule drugs have been extensively investigated [10–16]. Due to their high structural compatibility with the surface of a protein target, and their abilities to disrupt protein–protein interaction, peptides can be utilized as inhibitors that disrupt ACE2-PD and RBD binding [17, 18].

Computational approaches including molecular dynamics (MD) and computational protein design (CPD) have been utilized for designing peptide binders of RBD of the wuhan variant and other variants [19–22]. To inhibit ACE2 and RBD binding, CPD and MD were employed in our previous studies to design novel 25-mer peptide binders (SPB25), which were derived from ACE2-PD's α1 helix, that have better predicted SARS-CoV-2-RBD binding affinities ($\Delta G_{bind\ (MM\text{-}GBSA)}$) than ACE2 and 23-mer peptide binder (SBP1) [23, 24], which is the experimentally proven inhibitor of SARS-CoV-2-RBD [25]. Nonetheless, the knowledge on BIs between SPB25 and Omicron RBD as well as on whether our strategy, increasing favorable BIs between SPB25 and the conserved residues of RBD, can be used to create novel 25-mer peptides that have predicted $\Delta G_{bind\ (MM\text{-}GBSA)}$ to Omicron RBD better than ACE2 is limited.

Based on ACE2-PD's α1 helix (residues 21–45), this study used CPD (Rosetta) as well as MD (AMBER) to generate novel SPB25 that have better predicted $\Delta G_{bind\ (MM\text{-}GBSA)}$ to Omicron RBD than ACE2. We utilized the design strategy of increasing favorable BIs between SPB25 and the conserved residues of RBD. The designed SPB25 that have predicted $\Delta G_{bind\ (MM\text{-}GBSA)}$ to Omicron RBD better than ACE2 are promising peptides that may be utilized to inhibit BI between ACE2 and Omicron RBD.

Methods

Preparation of structures

The complex structure of ACE2 binding to Omicron RBD was from PDB ID: 7TN0 [26]. SPB25 structure (21 IEEQAKTFLDKFNHEAEDLFYQSSL 45) binding to Omicron RBD was extracted from ACE2-PD's α1 helix binding with Omicron RBD (PDB ID: 7TN0 [26]). These complexes were protonated at pH 7.4 (physiological pH) employing the H^{++} server [27]. AMBER18's LEaP module [28] was utilized to create the final complex structure.

Computational design of novel SPB25s

In this study, the design template for CPD (Rosetta [29]) was the structure of SPB25 in complex with Omicron RBD. This work employed the design strategy of increasing favorable BIs between the conserved residues of RBD (Y421, L455, F456, G485, F486 and Y489) [30] and residues 21–45 of ACE2 so that the designed SPB25 have better $\Delta G_{bind\ (MM\text{-}GBSA)}$ to Omicron RBD than ACE2. Designed positions were selected if favorable BIs could potentially be formed upon mutations between RBD's conserved residues and the side chains of designed positions. Employing CoupledMoves protocol [31, 32] of RosettaDesign module (Rosetta3.11) and beta_nov16 energy function, structures of selected designed residues/positions were

redesigned, repacked and minimized. Standard amino acids except G and P were allowed in each designed position. Additionally, residues within 10 Å of each designed position were repacked and energetically minimized. 400 runs were independently conducted for each design, producing 400 conformations of designed sequences, where some sequences may have various conformations. To calculate $\Delta G_{bind\ (Rosetta)}$ in Rosetta Energy Unit (REU) of each conformation, an interface analyzer [33, 34] module (Rosetta3.11) was used. $\Delta\Delta G_{bind\ (Rosetta)}$ upon mutation was determined by deducting $\Delta G_{bind\ (Rosetta)}$ of SPB25 from that of the designed conformation/sequence. MD was performed on designed conformations of all designed positions with $\Delta\Delta G_{bind\ (Rosetta)} < 0$ REU, and the molecular mechanics–generalized born surface area (MM-GBSA) method [35–37] was utilized to determine if their $\Delta G_{bind\ (MM\text{-}GBSA)}$ values are better than that of SPB25. The single mutants with better predicted $\Delta G_{bind\ (MM\text{-}GBSA)}$ than SPB25 were used to generate the double mutants of SPB25, and subsequently simulated to determine if their $\Delta G_{bind\ (MM\text{-}GBSA)}$ values are superior to that of SPB25.

MD and analyses

Complex structures of Omicron RBD binding to ACE2 and designed peptides were built in isomeric truncated octahedral boxes of TIP3P water utilizing the buffer distance of 13 Å as well as force field parameters of protein.ff14SB [38] and GLYCAM06j-1 [39] in AMBER18 [28]. To remove interactions that are unfavorable, all systems were energetically minimized, using the five-step procedure [23, 24, 40]. Employing different restraints on proteins, each minimization step contains 2,500 steps of steepest descent and 2,500 steps of conjugate gradient. In the first step, hydrogen atoms and water molecules were energetically minimized, while restraining proteins' heavy atoms using a force constant of 10 kcal/(mol $Å^2$). In the second, third and fourth steps of minimizations, force constants of 10, 5 and 1 kcal/(mol $Å^2$) were subsequently applied to restrain proteins' backbones, respectively. Lastly, the whole system was minimized without any restraining force. Subsequently, the GPU (CUDA) version of PMEMD module [41–43] was used for MD with the periodic boundary condition. To constrain all bonds with hydrogen atoms to allow the time step of 0.002 ps, SHAKE [44] was employed. To control each system's temperature, the Langevin dynamics method with a collision frequency of 1.0 ps^{-1} was used. For heating, the temperature of each system was increased from 0 K to 310 K in the NVT ensemble during 200 ps MD, while the backbones of the proteins were restrained with the force constant of 10 kcal/(mol $Å^2$). Each system was additionally equilibrated in the NVT ensemble without any restraining force at 310 K for 300 ps. In the production run, each system was subject to MD in the NPT ensemble at 310 K and 1 atm for 100 ns.

The structural stabilities of all systems were measured based on their Root Mean Square Deviation (RMSD) values with respect to their minimized structures. Further analyses were conducted on 80–100 ns trajectories, which have stable RMSD values. To predict each complex's binding affinity, the MM-GBSA technique was utilized to compute their total binding free energies [$\Delta G_{bind\ (MM\text{-}GBSA)}$]. The MM-GBSA method uses the following equation to compute $\Delta G_{bind\ (MM\text{-}GBSA)}$.

$$\Delta G_{bind} = G_{complex} - G_{receptor} - G_{ligand}$$

$$= \Delta E_{MM} + \Delta G_{polar(GB)} + \Delta G_{non-polar(SA)} - T\Delta S$$

$$= \Delta E_{vdw} + \Delta E_{ele} + \Delta G_{polar(GB)} + \Delta G_{non-polar(SA)} - T\Delta S,$$

where ΔG_{bind} is the total binding free energy of the system that is defined as the difference between the free energies of the complex ($G_{complex}$), the receptor ($G_{receptor}$), and the ligand

(G_{ligand}). ΔG_{bind} is calculated as the sum of the molecular mechanics free energy (ΔE_{MM}), the solvation free energy consisting of polar ($\Delta G_{polar(GB)}$) and nonpolar contributions ($\Delta G_{non\text{-}polar\ (SA)}$), and the entropy ($-T\Delta S$) in the gas phase. The ΔE_{MM} term comprises ΔE_{vdw} (van der Waals) and ΔE_{ele} (electrostatic). The polar and non-polar contributions are estimated by the Generalized-Born (GB) implicit solvation model and the molecular solvent accessible surface area (SASA). In this work, the entropic contribution ($-T\Delta S$) was not included in the calculation of ΔG_{bind} because the nmode module of AMBER predicts this term with high computational cost but not high accuracy [45, 46].

Designed SPB25s with $\Delta G_{bind\ (MM\text{-}GBSA)}$ better than ACE2 were selected for additional analyses including BIs and per-residue free energy decomposition (PFED). Hydrogen-bond (H-bond) occupations were determined to identify H-bonds of all systems. The following rules were employed to consider an occurrence of a H-bond: (i) a proton donor-acceptor distance $\leq$3.5 Å and (ii) a donor-H-acceptor bond angle $\geq$120˚. In this work, three levels of occupations were defined: (i) strong H-bonds with H-bond occupations $>$ 75%, (ii) medium H-bonds with 75% $\geq$ H-bond occupations $>$ 50%, and (iii) weak H-bond interactions with 50% $\geq$ H-bond occupations $>$ 25% [23, 24, 40, 47]. To measure the peptide helicity of each system, Define Secondary Structure of Protein (DSSP) was utilized to compute the percent helicity from the summation of the percentage of α-, π- and 3-10-helix structures [48].

Results

Computational design of SPB25s of Omicron RBD

The template structure of SPB25 binding to Omicron RBD (Fig 1) was extracted from the structure of ACE2-PD's α1 helix binding to Omicron RBD (PDB ID: 7TN0). Our design strategy is enhancing favorable BIs between the conserved residues of RBD (Y421, L455, F456, G485, F486 and Y489) [30] and SPB25. Designed positions of SPB25 were selected if favorable BIs could potentially form upon mutations between their side chains and the conserved residues of RBD. Q4(24), T7(27), F8(28), D10(30), K11(31) and H14(34) were chosen based on this criterion. Standard amino acids, except G and P due to their low occurring frequencies in an α-helix, were allowed in each designed position. In addition, P could cause the formation of a kink that can destabilize a helix [49]. Using these designed positions and amino acid types as inputs to Rosetta, 52 designed SPB25s that have single mutations (S1 Table) were produced. Sixteen designed SPB25s with better $\Delta G_{bind\ (Rosetta)}$ than SPB25 ($\Delta\Delta G_{bind\ (Rosetta)} < 0$ REU) were simulated to determine if their $\Delta G_{bind\ (MM\text{-}GBSA)}$ calculated by the more accurate MM-GBSA method were better than that of SPB25 ($\Delta\Delta G_{bind\ (MM\text{-}GBSA)} < 0$ kcal/mol). $SPB25_{Q4C}$, $SPB25_{T7L}$, $SPB25_{T7W}$, $SPB25_{F8A}$, $SPB25_{D10L}$, $SPB25_{D10M}$, $SPB25_{D10R}$, $SPB25_{K11A}$, $SPB25_{K11L}$, $SPB25_{K11M}$, $SPB25_{K11N}$, $SPB25_{K11Q}$, $SPB25_{K11V}$, $SPB25_{K11W}$, $SPB25_{K11Y}$, and $SPB25_{H14V}$ are designed peptides with $\Delta\Delta G_{bind\ (MM\text{-}GBSA)} < 0$ kcal/mol.

MD and calculations of binding free energies

Complex structures of all 16 designed 25-mer peptides, SPB25 and ACE2 binding to Omicron RBD were simulated for 100 ns. Using the MM-GBSA technique, $\Delta G_{bind\ (MM\text{-}GBSA)}$ of all complexes were computed to assess whether $\Delta G_{bind\ (MM\text{-}GBSA)}$ of designed SPB25s are better than that of SPB25. To determine the stabilities of each system, Root Mean Square Deviation (RMSD) of all and backbone atoms were computed (S1 Fig). RMSD plots show that it likely took around 80 ns for each system to reach equilibrium. As a result, further analyses were conducted on the 80–100 ns trajectory of each system.

The MM-GBSA technique was utilized to compute $\Delta G_{bind\ (MM\text{-}GBSA)}$ of each system from its 80–100 ns trajectory. Table 1 illustrates that $\Delta G_{bind\ (MM\text{-}GBSA)}$ of ACE2 and SPB25 binding

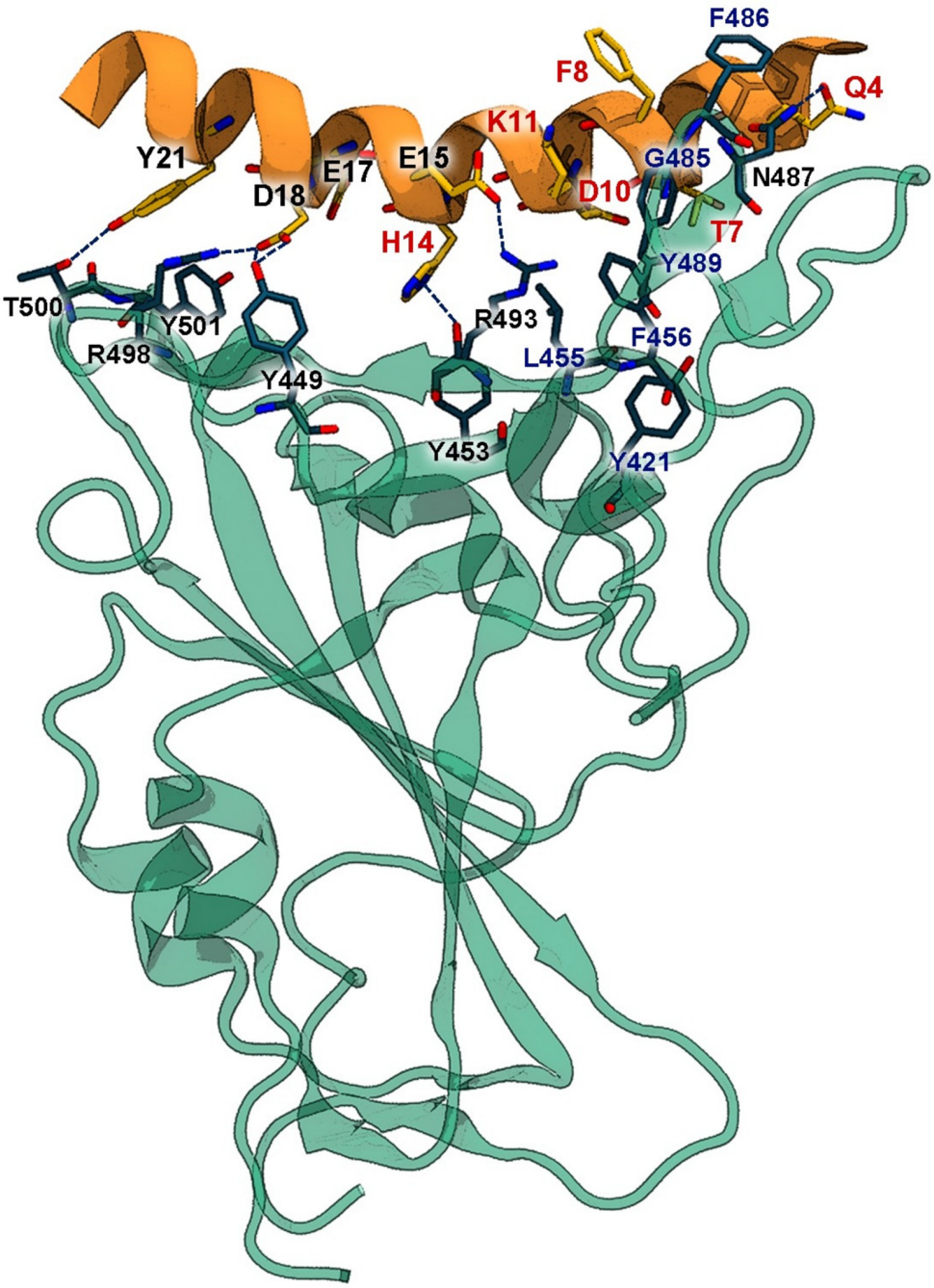

Fig 1. The design template structure of SPB25 binding to Omicron RBD. Omicron RBD and SPB25 are displayed in cyan and orange, respectively. Conserved residues of RBD and the designed positions are labelled in blue and red, respectively.

https://doi.org/10.1371/journal.pone.0292589.g001

to Omicron RBD are −87.9 ± 0.5, and −71.6 ± 0.5 kcal/mol, respectively. $\Delta G_{bind\ (MM\text{-}GBSA)}$ of seven designed SPB25s, out of 16 designed SPB25s with single mutations, such as $SPB25_{T7L}$, $SPB25_{F8A}$, $SPB25_{K11A}$, $SPB25_{K11L}$, $SPB25_{K11M}$, $SPB25_{K11Q}$, and $SPB25_{K11V}$ are better than that of SPB25 with $\Delta\Delta G_{bind\ (MM\text{-}GBSA)}$ of −3.1 ± 0.8, −14.9 ± 0.8, −1.6 ± 0.7, −9.2 ± 0.7, −7.8 ± 0.8, −5.8 ± 0.8, and −9.6 ± 0.9 kcal/mol, respectively. The total of 11 and 5 designed SPB25s

Table 1. Predicted binding free energies, by Rosetta and the MM-GBSA technique, to Omicron RBD of ACE2, SPB25 and designed SPB25 that were chosen for simulations.

System	$\Delta\Delta G_{bind\ (Rosetta)}$ [a] (REU)	$\Delta G_{bind\ (MM\text{-}GBSA)}$ (kcal/mol)	$\Delta\Delta G_{bind\ (MM\text{-}GBSA)}$ [b] (kcal/mol)
ACE2	-	−87.9 ± 0.5	−16.3 ± 0.7
SPB25	-	−71.6 ± 0.5	0.0 ± 0.7
$SPB25_{Q4C}$	−0.2	−65.7 ± 0.7	5.9 ± 0.9
$SPB25_{T7L}$	−1.9	−74.7 ± 0.6	−3.1 ± 0.8
$SPB25_{T7W}$	−0.9	−61.6 ± 0.7	10.0 ± 0.9
$SPB25_{F8A}$	−0.2	−86.5 ± 0.6	−14.9 ± 0.8
$SPB25_{D10L}$	−0.8	−70.1 ± 0.8	1.5 ± 0.9
$SPB25_{D10M}$	−1.7	−70.0 ± 0.7	1.6 ± 0.9
$SPB25_{D10R}$	−2.4	−69.8 ± 0.5	1.8 ± 0.7
$SPB25_{K11A}$	−0.4	−73.2 ± 0.5	−1.6 ± 0.7
$SPB25_{K11L}$	−0.6	−80.8 ± 0.5	−9.2 ± 0.7
$SPB25_{K11M}$	−0.1	−79.4 ± 0.6	−7.8 ± 0.8
$SPB25_{K11N}$	−0.8	−66.2 ± 0.4	5.4 ± 0.6
$SPB25_{K11Q}$	−0.1	−77.4 ± 0.6	−5.8 ± 0.8
$SPB25_{K11V}$	−1.9	−81.2 ± 0.7	−9.6 ± 0.9
$SPB25_{K11W}$	−0.8	−61.3 ± 0.4	10.3 ± 0.6
$SPB25_{K11Y}$	−1.1	−61.9 ± 0.5	9.7 ± 0.7
$SPB25_{H14V}$	−0.7	−65.4 ± 0.5	6.2 ± 0.7
$SPB25_{T7L/F8A}$	−0.8	−84.6 ± 0.7	−13.0 ± 0.9
$SPB25_{T7L/K11A}$	0.9	−92.4 ± 0.4	−20.8 ± 0.6
$SPB25_{T7L/K11L}$	−2.1	−95.7 ± 0.5	−24.1 ± 0.7
$SPB25_{T7L/K11M}$	−0.1	−57.0 ± 0.7	14.6 ± 0.9
$SPB25_{T7L/K11Q}$	−1.1	−78.1 ± 0.5	−6.5 ± 0.7
$SPB25_{T7L/K11V}$	−1.9	−79.0 ± 0.6	−7.4 ± 0.8
$SPB25_{F8A/K11A}$	−0.1	−71.0 ± 0.4	0.6 ± 0.6
$SPB25_{F8A/K11L}$	−2.8	−73.7 ± 0.5	−2.1 ± 0.7
$SPB25_{F8A/K11M}$	−0.8	−74.7 ± 0.5	−3.1 ± 0.7
$SPB25_{F8A/K11Q}$	−2.0	−76.1 ± 0.6	−4.5 ± 0.8
$SPB25_{F8A/K11V}$	−2.1	−77.8 ± 0.7	−6.2 ± 0.9
$SPB25_{T7L/F8A/K11A}$	0.4	−51.6 ± 0.8	20.0 ± 0.9
$SPB25_{T7L/F8A/K11L}$	−3.1	−59.6 ± 0.4	12.0 ± 0.6
$SPB25_{T7L/F8A/K11M}$	−1.6	−59.1 ± 0.6	12.5 ± 0.8
$SPB25_{T7L/F8A/K11Q}$	−1.5	−76.8 ± 0.6	−5.2 ± 0.8
$SPB25_{T7L/F8A/K11V}$	−1.9	−67.0 ± 0.5	4.6 ± 0.7

[a] The difference between $\Delta G_{bind\ (Rosetta)}$ of a system and that of SPB25.

[b] The difference between $\Delta G_{bind\ (MM\text{-}GBSA)}$ of a system and that of SPB25.

https://doi.org/10.1371/journal.pone.0292589.t001

containing double and triple mutations were also built based on the seven designed SPB25s with single mutations, employing Rosetta. They were subject to MD, and their values of $\Delta G_{bind\ (MM\text{-}GBSA)}$ were predicted by the MM-GBSA technique. In terms of designed SPB25s that contain double mutations, $\Delta G_{bind\ (MM\text{-}GBSA)}$ of $SPB25_{T7L/F8A}$, $SPB25_{T7L/K11A}$, $SPB25_{T7L/K11L}$, $SPB25_{T7L/K11Q}$, $SPB25_{T7L/K11V}$, $SPB25_{F8A/K11L}$, $SPB25_{F8A/K11M}$, $SPB25_{F8A/K11Q}$, and $SPB25_{F8A/K11V}$ are better than that of SPB25 with the $\Delta\Delta G_{bind\ (MM\text{-}GBSA)}$ of −13.0 ± 0.9, −20.8 ± 0.6, −-24.1 ± 0.7, −6.5 ± 0.7, −7.4 ± 0.8, −2.1 ± 0.7, −3.1 ± 0.7, −4.5 ± 0.8, and −6.2 ± 0.9 kcal/mol, respectively. Moreover, the predicted binding affinities of $SPB25_{T7L/K11A}$ ($\Delta G_{bind\ (MM\text{-}GBSA)}$ =

−92.4 ± 0.4 kcal/mol) and SPB25$_{T7L/K11L}$ ($\Delta G_{bind\ (MM\text{-}GBSA)}$ = −95.7 ± 0.5 kcal/mol) are better than that of ACE2 ($\Delta G_{bind\ (MM\text{-}GBSA)}$ = −87.9 ± 0.5 kcal/mol). For designed SPB25s with triple mutations, only $\Delta G_{bind\ (MM\text{-}GBSA)}$ of SPB25$_{T7L/F8A/K11Q}$ is better than that of SPB25 with $\Delta\Delta G_{bind\ (MM\text{-}GBSA)}$ of −5.2 ± 0.8 kcal/mol.

The binding free energy components of designed SPB25s with better $\Delta G_{bind\ (MM\text{-}GBSA)}$ than ACE2

The binding free energy components of ACE2, SPB25 and two designed SPB25s with better predicted $\Delta G_{bind\ (MM\text{-}GBSA)}$ to Omicron RBD than ACE2 are shown in Fig 2. The main contributor to the favorable $\Delta G_{bind\ (MM\text{-}GBSA)}$ to Omicron RBD of ACE2, SPB25, SPB25$_{T7L/K11A}$, and SPB25$_{T7L/K11L}$ is the electrostatic interaction term. Other terms that also favorably contribute to $\Delta G_{bind\ (MM\text{-}GBSA)}$ are the non-polar solvation and van der Waals energy terms. The term that unfavorably contributes to $\Delta G_{bind\ (MM\text{-}GBSA)}$ is the polar solvation term.

SPB25$_{T7L/K11A}$ and SPB25$_{T7L/K11L}$ are the designed 25-mer peptides that have the best $\Delta G_{bind\ (MM\text{-}GBSA)}$ to Omicron RBD ($\Delta G_{bind\ (MM\text{-}GBSA)}$ values of −92.4 ± 0.4 and −95.7 ± 0.5 kcal/mol, respectively). Their $\Delta G_{bind\ (MM\text{-}GBSA)}$ are better than that of SPB25 by 20.8 ± 0.6 and 24.1 ± 0.7 kcal/mol, respectively, and better than that of ACE2 by 4.5 ± 0.6 and 7.8 ± 0.7 kcal/mol, respectively. As compared to those of SPB25, the major contributions to the favorable BI of SPB25$_{T7L/K11A}$ and SPB25$_{T7L/K11L}$ to Omicron RBD are the increases in their favorable electrostatic interaction, van der Waals energy, and non-polar solvation terms. Nevertheless, their unfavorable polar solvation terms are higher than that of SPB25.

Elucidation of important binding residues (IBRs) of designed SPB25s with $\Delta G_{bind\ (MM\text{-}GBSA)}$ better than ACE2

To elucidate IBRs to Omicron RBD, PFED of two designed 25-mer peptides with $\Delta G_{bind\ (MM\text{-}GBSA)}$ better than ACE2 were computed (Fig 3). Residues that have the total energy contribution (TEC) better than −1.0 kcal/mol were identified as IBRs. In terms of residues 21–45 of the α1 helix of ACE2, Q24, T27, F28, K31, H34, E35, Y41, and L45 were identified as IBRs to Omicron RBD. The predicted IBRs of SPB25 are E3(23), K6(26), T7(27), D10(30), K11(31), H14(34), E17(37), D18(38), F20(40), and Y21(41). The total IBRs of SPB25$_{T7L/K11A}$ (12) and SPB25$_{T7L/K11L}$ (11) are more than those of residues 21–45 of the α1 helix of ACE2 (8) and SPB25 (10). Eight residues of these two designed 25-mer peptides have high predicted $\Delta G_{bind\ (MM\text{-}GBSA)}$ (better than -2 kcal/mol) including Q4, L7, F8, A11/L11, H14 (the highest binding affinity residue), E15, D18 and Y21.

In terms of TECs of SPB25$_{T7L/K11A}$, the T7L/K11A mutations were predicted to favorably enhance TECs of residue 7 from −2.5 and −2.4 kcal/mol in ACE2 and SPB25, respectively to −3.4 in SPB25$_{T7L/K11A}$. TEC of residue 11 was favorably enhanced from −1.1 kcal/mol in ACE2 to −2.2 kcal/mol in SPB25$_{T7L/K11A}$, while it was unfavorably reduced from −2.9 kcal/mol in SPB25 to −2.2 kcal/mol in SPB25$_{T7L/K11A}$. Nonetheless, TECs of other residues including I1, Q4, A5, F8, D10, H14, D18, Y21 and L25 were favorably enhanced from −0.2, −2.9, −0.1, −1.7, −0.2, −5.8, 0.6, −2.2 and −1.1 kcal/mol in ACE2 and 1.1, −0.6, 0.0, −0.2, −1.4, −4.7, −3.4, −1.1 and −0.7 kcal/mol in SPB25 to −1.4, −3.9, −1.1, −3.5, −1.8, −6.8, −4.7, −4.0 and −1.7 kcal/mol in SPB25$_{T7L/K11A}$, respectively. Additionally, TEC of E15 was also favorably enhanced from −0.2 kcal/mol in SPB25 to −3.5 kcal/mol in SPB25$_{T7L/K11A}$.

In terms of TECs of SPB25$_{T7L/K11L}$, the T7L/K11L mutations were predicted to favorably enhance TECs of residues 7 and 11 from −2.5 and −1.1 kcal/mol in ACE2 and −2.4 and −2.9 kcal/mol in SPB25 to −2.6 and −3.3 kcal/mol in SPB25$_{T7L/K11L}$, respectively, Additionally, TECs of A5, F8, L9, H14, D18 and Y21 were also favorably enhanced from −0.1, −1.7, −0.2,

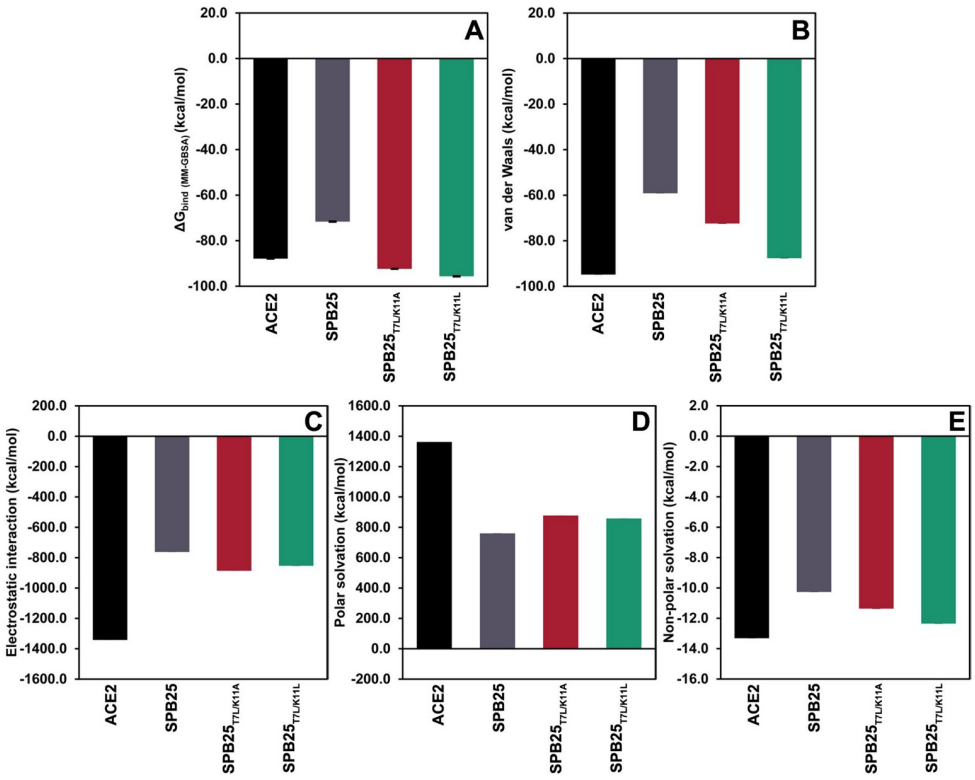

Fig 2. The binding free energy components of ACE2, SPB25 and designed SPB25s in complex with Omicron RBD. A) $\Delta G_{bind\ (MM\text{-}GBSA)}$, B) van der Waals energy, C) electrostatic interaction D) polar solvation and E) non-polar solvation.

https://doi.org/10.1371/journal.pone.0292589.g002

−5.8, 0.6 and −2.2 kcal/mol in ACE2 and 0.0, −0.2, −0.3, −4.7, −3.4 and −1.1 kcal/mol in SPB25 to −1.4, −6.8, −1.1, −7.2, −5.5 and −5.4 kcal/mol in $SPB25_{T7L/K11L}$, respectively. Moreover, TECs of Q4, E15 and L25 were favorably enhanced from −0.6, −0.2 and −0.7 kcal/mol in SPB25 to −2.1, −3.2 and −1.1 kcal/mol in $SPB25_{T7L/K11L}$.

H-bond and π interactions of designed SPB25s that have better $\Delta G_{bind\ (MM\text{-}GBSA)}$ than ACE2

To elucidate important H-bonds, cation-π, anion-π, π-π, σ-π and alkyl-π interactions for the binding of ACE2, SPB25 and the best 25-mer designed peptides to Omicron RBD, H-bond occupations and π interactions were investigated as shown in Tables 2 and S2. H34, Y83 and K353 of ACE2 had strong H-bonds with the backbones of R493, N487 and G502 of Omicron RBD, respectively. S19, Q24, E35, D38 and D355 of ACE2 had medium H-bonds with A475, N487, R493, Y449 and T500 of Omicron RBD. Additionally, there were weak H-bonds between S19, H34, E35 and Y41 of ACE2 and A475, S494, R493 and T500 of Omicron RBD, respectively. For the π interactions between Omicron RBD and ACE2, there was a cation-π interaction between K31 of ACE2 and Y489 of Omicron RBD. F28, H34, Y41 and Y83 of ACE2 had π-π interactions with F486, Y453, Y501 and F486 of Omicron RBD. There was also a σ-π interaction between H34 of ACE2 and R493 of Omicron RBD. In addition, K31, H34, L79, M82 and K353 of ACE2 had alkyl-π interactions with Y489, R493, F486, F486, Y501 and H505 of Omicron RBD, respectively.

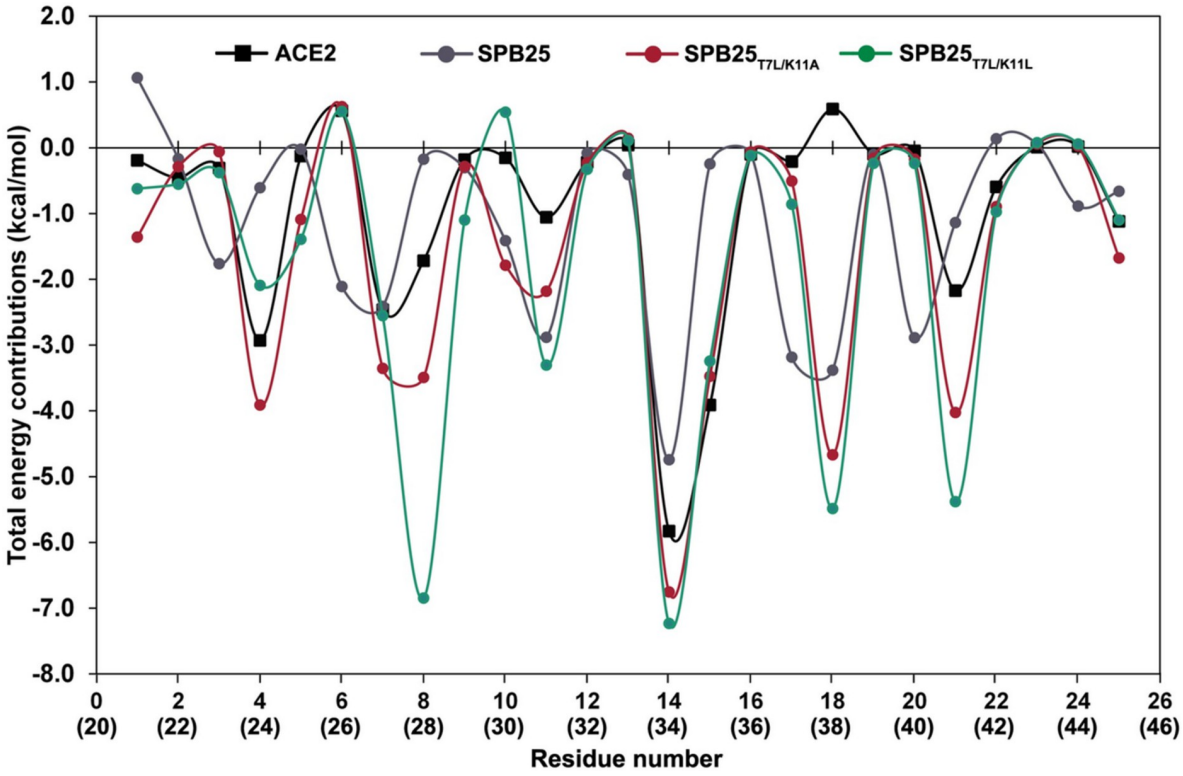

Fig 3. PFED of the best designed 25-mer peptides, SPB25, and ACE2 in binding to Omicron RBD. ACE2's residue numbers are shown in parenthesis.

https://doi.org/10.1371/journal.pone.0292589.g003

For H-bond and π interactions between SPB25 and Omicron RBD, D10, H14, E17 and D18 of SPB25 had six strong H-bonds with N417, R493, R403 and R493 of Omicron RBD. There were also medium H-bonds between T7, D10 and E17 of SPB25 and Y473, Y421 and R403 of Omicron RBD, respectively. Additionally, there were two weak H-bonds between E17 and E18 of SPB25 and R403 and R493 of Omicron RBD. In terms of π-interactions, H14 and Y21 of SPB25 had two cation-π interactions with R493 of Omicron RBD. There were four π-π interactions between H14 and F20 of SPB25 and F456, Y489, Y501 and H505 of Omicron RBD. Moreover, K11 and H14 of SPB25 had alkyl-π interactions with Y489 and L455 of Omicron RBD, respectively.

Fig 4 illustrates key predicted BIs between the two best designed 25-mer peptides and Omicron RBD. The overall binding poses of these two designed SPB25s and ACE2 binding to omicron RBD are relatively similar. In terms of predicted interactions to Omicron RBD, the total no. of H-bonds of $SPB25_{T7L/K11A}$ is higher than those of ACE2 and SPB25. Additionally, no. of strong H-bonds of $SPB25_{T7L/K11A}$ is higher than those of ACE2 and SPB25, supporting the result that its $\Delta G_{bind\ (MM\text{-}GBSA)}$ is better than ACE2 and SPB25. D18 of $SPB25_{T7L/K11A}$ had four strong H-bonds with R498 and Y501 of Omicron RBD. Additionally, H14 of $SPB25_{T7L/K11A}$ had three strong H-bonds with R493 and Y501 of Omicron RBD. D10 and E15 of $SPB25_{T7L/K11A}$ had four medium H-bonds with R403 and R493 of Omicron RBD. Furthermore, other residues such as Q4 and Y21 had H-bonds with Omicron RBD. In terms of π interactions between $SPB25_{T7L/K11A}$ and Omicron RBD, no. of π interactions of $SPB25_{T7L/K11A}$ is more than that of SPB25. H14 of $SPB25_{T7L/K11A}$ had two cation-π interactions with R403 and R493 of Omicron RBD. In addition, there were five π-π interactions (F8 –Y489, H14 –Y501, H14 –

Table 2. No. of H-bond and π interactions of ACE2, SPB25 and designed SPB25s involved in binding to Omicron RBD.

System	No. of H-bonds			Residue that forms a H-bond with Omicron RBD	π interaction				
	Strong	Medium	Weak		Cation-π	Anion-π	π-π	σ-π	Alkyl-π
ACE2	4	7	5	S19, Q24, H34, E35, D38, Y41, Y83, K353, D355	K31@NZ–Y489	-	F28 – F486 H34 – Y453 Y41 – Y501 Y83 – F486	H34 – R493@HB3	K31 –Y489 H34 –R493 L79 –F486 M82 – F486 K353 – Y501 K353 – H505
SPB25	6	3	2	T7, D10, H14, E17, D18	H14 – R493@NH1 Y21 – R493@NH2	-	H14 – F456 H14 – Y489 F20 – Y501 F20 – H505	-	K11 –Y489 H14 –L455
$SPB25_{T7L/K11A}$	7	4	9	Q4, D10, H14, E15, D18, Y21	H14 – R403@NH1 H14 – R493@NH2	-	F8 –Y489 H14 – Y501 H14 – H505 Y21 – Y501 Y21 – H505	Y21 – Y501@HA	A5 –Y489 H14 –R493
$SPB25_{T7L/K11L}$	6	1	6	Q4, H14, E15, D18, Y21	-	E17@OE1 – H505 E17@OE2 – H505	F8 –F456 F8 –Y473 F8 –Y489 H14 – Y453 H14 – Y495 H14 – H505 Y21 – Y501 Y21 – H505	Y21 – Y501@HA	A5 –Y473 A5 –Y489 L7 –F456 F8 –L455 F8 –A475 L9 –Y489 H14 –R493

https://doi.org/10.1371/journal.pone.0292589.t002

H505, Y21 –Y501 and Y21 –H505), one σ-π interaction (Y21 –Y501@HA), and two alkyl-π interactions (A5 –Y489 and H14 –R493) between $SPB25_{T7L/K11A}$ and Omicron RBD.

Regarding the predicted BIs of $SPB25_{T7L/K11L}$, the total no. of H-bonds of $SPB25_{T7L/K11L}$ is higher than that of SPB25 and lower than that of ACE2. However, no. of π interactions of $SPB25_{T7L/K11L}$ is higher than those of ACE2 and SPB25. H14 and D18 of $SPB25_{T7L/K11L}$ had six strong H-bonds with R493, R498 and Y501 of Omicron RBD. Moreover, there was one medium H-bond between E15 of $SPB25_{T7L/K11L}$ and R493 of Omicron RBD. Additionally, Q4 and Y21 had H-bonds with Omicron RBD. The mutated residue L7 of $SPB25_{T7L/K11L}$ also had alkyl-π interaction with F456 of Omicron RBD, while T27 of ACE2 and T7 of SPB25 had no π interaction with Omicron RBD. Furthermore, other residues had two anion-π interactions (E17@OE1 –H505 and E17@OE2 –H505), eight π-π interactions (F8 –F456, F8 –Y473, F8 –Y489, H14 –Y453, H14 –Y495, H14 –H505, Y21 –Y501 and Y21 –H505), one σ-π interaction (Y21 –Y501@HA), and seven alkyl-π interactions (A5 –Y473, A5 –Y489, L7 –F456, F8 –L455, F8 –A475, L9 –Y489, H14 –R493) between $SPB25_{T7L/K11L}$ and Omicron RBD.

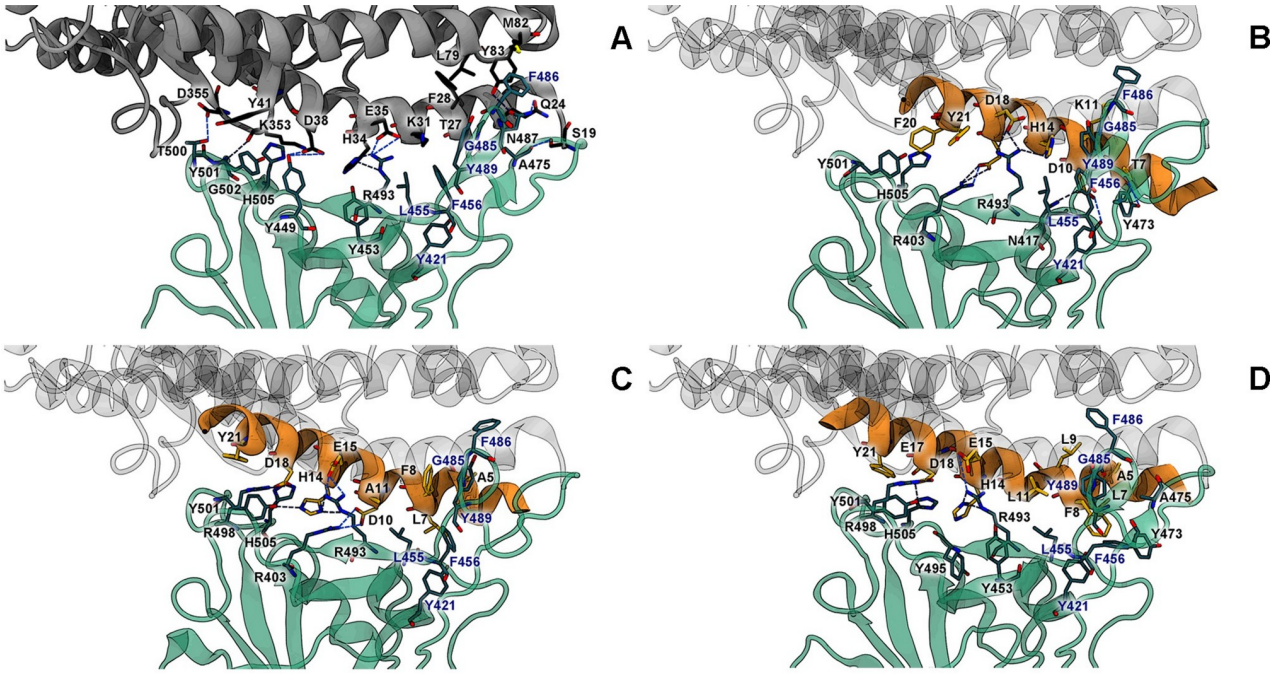

Fig 4. Key BIs between Omicron RBD (cyan) and A) ACE2, B) SPB25, C) $SPB25_{T7L/K11A}$, or D) $SPB25_{T7L/K11L}$. The structures closest to the average structures from the 80–100 ns MD trajectories of SPB25 and designed SPB25s (orange) were superimposed with that of ACE2 (grey). Key salt bridges and H-bonds (H-bond occupations > 25%) are represented as blue dashed lines.

https://doi.org/10.1371/journal.pone.0292589.g004

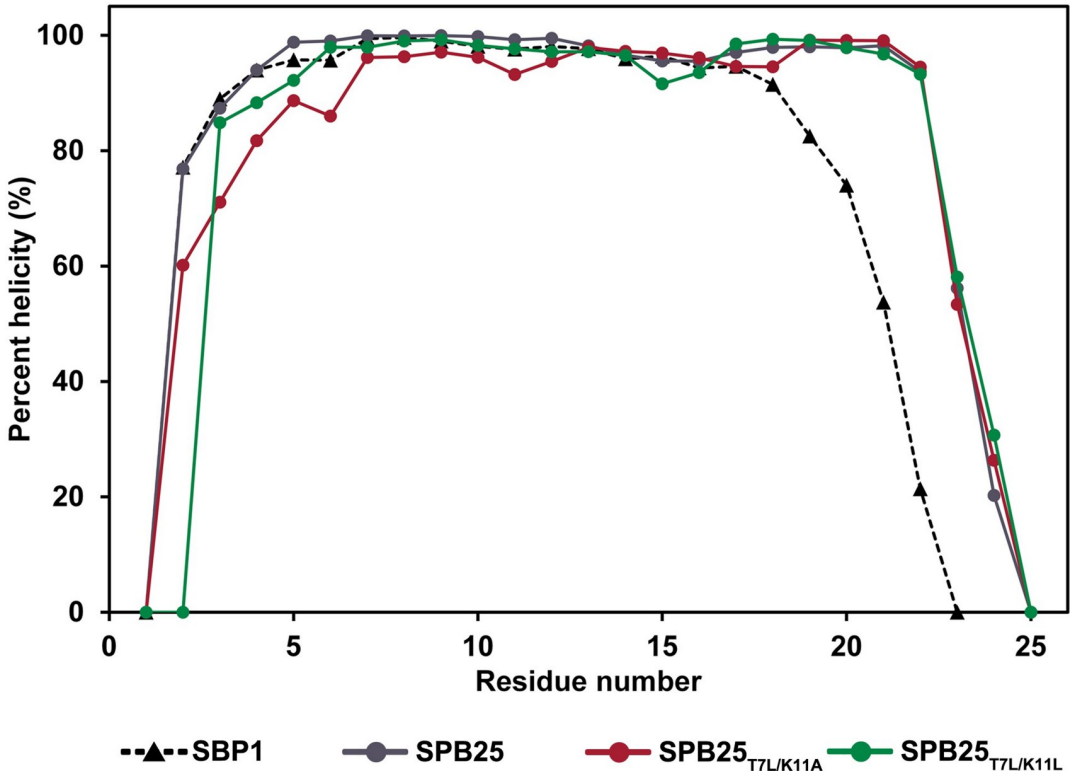

Fig 5. The percent helicities in water of SBP1 [23], SPB25 and designed SPB25s with better $\Delta G_{bind\ (MM\text{-}GBSA)}$ than ACE2.

https://doi.org/10.1371/journal.pone.0292589.g005

Peptide helicities of designed SPB25s with better $\Delta G_{bind\ (MM\text{-}GBSA)}$ than ACE2

Figs 5 and S2 show the percent helicities and structural stabilities (RMSD plots) in water of designed 25-mer peptides with better predicted bind affinities to Omicron RBD than ACE2, respectively. The percent helicities of the N- and C-termini of the two best designed peptides are lower than those of middle residues due to their high flexibilities. Overall trends of percent helicities of $SPB25_{T7L/K11A}$ and $SPB25_{T7L/K11L}$ are slightly higher than those of SBP1.

Discussion

The omicron variant (B.1.1.529) was the important variant of concern that was responsible for the COVID-19 pandemic. Similar to other variants, Omicron RBD firstly attaches to ACE2-PD to enter human cells. Disrupting BIs between ACE2-PD and Omicron RBD to prevent coronavirus from infecting and destroying human cells is a promising COVID-19 therapy. Since peptides have more similar interactions to native protein-protein interactions and functional groups than small molecules, which can be ineffective in disrupting large protein-binding interfaces[17, 18], peptides can be employed as inhibitors of SARS-CoV-2 to inhibit protein-protein interactions at their binding interfaces.

To design novel 25-mer peptides with high potential to bind to Omicron RBD better than ACE2, we employed CPD, using the residues 21–45 of ACE2-PD's α1 helix as a template, and MD. The design strategy of this study was increasing favorable BIs between SPB25 and the conserved residues of RBD (Y421, L455, F456, G485, F486 and Y489). Q4(24), T7(27), F8(28), D10(30), K11(31) and H14(34) were chosen as designed positions because their side chains are in the orientations that can possibly form favorable BIs with Omicron RBD upon mutations. Standard amino acids, except G and P, were allowed for all designed positions. After CPD by Rosetta, 52 designed SPB25s that have single mutations were generated. Sixteen designed SPB25s with superior $\Delta G_{bind\ (Rosetta)}$ to SPB25 ($\Delta\Delta G_{bind\ (Rosetta)} < 0$ REU) were simulated, and their $\Delta G_{bind\ (MM\text{-}GBSA)}$ were computed by the MM-GBSA technique and compared to those of SPB25 and ACE2. The predicted binding affinity of ACE2 to Omicron RBD ($\Delta G_{bind\ (MM\text{-}GBSA)}$ = −87.9 ± 0.5 kcal/mol) is better than that of SARS-CoV-2-RBD ($\Delta G_{bind\ (MM\text{-}GBSA)}$ = −71.2 ± 0.4 kcal/mol) [23], supporting the experimental findings that ACE2 bound to Omicron RBD (K_D = 38.9 ± 10.5 nM) with higher affinity than the wild type (K_D = 75.5 ± 2.1 nM) [9]. Additionally, the predicted binding affinity of SPB25 to Omicron RBD (−71.6 ± 0.5 kcal/mol) is better than that of SARS-CoV-2-RBD (−60.3±0.4 kcal/mol) [23], suggesting that it should be able to experimentally bind to Omicron RBD better than that of the wild type. However, the predicted binding affinity to Omicron RBD of SPB25 is worse than that of ACE2 probably because no. of IBRs of ACE2 to Omicron RBD is significantly more than SPB25, which also includes those in the α2-helix and the linker of the β3- and β4-sheets.

The predicted binding affinities to Omicron RBD of seven designed 25-mer peptides such as $SPB25_{T7L}$, $SPB25_{F8A}$, $SPB25_{K11A}$, $SPB25_{K11L}$, $SPB25_{K11M}$, $SPB25_{K11Q}$, and $SPB25_{K11V}$ are better than that of SPB25 with $\Delta\Delta G_{bind\ (MM\text{-}GBSA)}$ of −3.1 ± 0.8, −14.9 ± 0.8, −1.6 ± 0.7, −-9.2 ± 0.7, −7.8 ± 0.8, −5.8 ± 0.8, and −9.6 ± 0.9 kcal/mol, respectively. They were subsequently used to create 11 and 5 designed peptides that have double and triple mutations, respectively, using Rosetta. Subsequently, all designed peptides were subjected to MD, and their $\Delta G_{bind\ (MM\text{-}GBSA)}$ were calculated. For the designed 25-mer peptides with double mutations, the predicted binding affinities to Omicron RBD of $SPB25_{T7L/F8A}$, $SPB25_{T7L/K11A}$, $SPB25_{T7L/K11L}$, $SPB25_{T7L/K11Q}$, $SPB25_{T7L/K11V}$, $SPB25_{F8A/K11L}$, $SPB25_{F8A/K11M}$, $SPB25_{F8A/K11Q}$, and $SPB25_{F8A/K11V}$ are better than that of SPB25 with $\Delta\Delta G_{bind\ (MM\text{-}GBSA)}$ of −13.0 ± 0.9, −20.8 ± 0.6, −-24.1 ± 0.7, −6.5 ± 0.7, −7.4 ± 0.8, −2.1 ± 0.7, −3.1 ± 0.7, −4.5 ± 0.8, and −6.2 ± 0.9 kcal/mol,

respectively. In terms of designed SPB25s containing triple mutations, the predicted binding affinity to Omicron RBD of $SPB25_{T7L/F8A/K11Q}$ is better than that of SPB25 with $\Delta\Delta G_{bind\ (MM\text{-}GBSA)}$ of −5.2 ± 0.8 kcal/mol. Most importantly, the predicted binding affinities to Omicron RBD of two designed peptides ($SPB25_{T7L/K11A}$ and $SPB25_{T7L/K11L}$) are better than that of ACE2 by 4.5 ± 0.6 and 7.8 ± 0.7 kcal/mol, respectively, suggesting that they should be able to experimentally bind to Omicron RBD better than ACE2. Furthermore, the binding positions and orientations to Omicron RBD of all designed SPB25s and those of residues 21–45 of ACE2-PD's α1 helix are relatively similar, suggesting that they could potentially inhibit Omicron RBD and ACE2-PD binding.

Our best designed SPB25 is $SPB25_{T7L/K11L}$ since its $\Delta G_{bind\ (MM\text{-}GBSA)}$ is better than those of ACE2, SPB25 and $SPB25_{T7L/K11A}$. This result is supported by the fact that no. of π interactions (including A5, L7, F8, L9, H14, E17 and Y21) is higher than those of ACE2, SPB25 and $SPB25_{T7L/K11A}$. Its total no. of H-bonds (including Q4, H14, E15, D18 and Y21) is more than that of SPB25 and lower than that of ACE2. Nonetheless, its no. of strong H-bonds is higher than that of ACE2. The results from PFED suggest Q4, A5, L7, F8, L9, A11, H14, E15, D18, Y21 and L25 as IBRs. Moreover, the T7L/K11L mutation was predicted to favorably enhance TEC of residue 7 and 11 and other residues such as A5, F8, L9, H14, D18 and Y21 as compared to those of ACE2 and SPB25.

$\Delta G_{bind\ (MM\text{-}GBSA)}$ of $SPB25_{T7L/K11A}$ is better than those of SPB25 and ACE2, and this finding is supported by the fact that the total no. of H-bonds (including Q4, D10, H14, E15, D18 and Y21) is higher than those of ACE2 and SPB25. Its no. of strong H-bonds (including H14 and D18) is also higher than those of ACE2 and SPB25. Furthermore, its total no. of π interactions (including A5, F8, H14 and Y21) is more than that of SPB25. PFED analysis suggests I1, Q4, A5, L7, F8, D10, A11, H14, E15, D18, Y21 and L25 as IBRs. Additionally, the T7L/K11A mutation was predicted to bring about substantial enhancement in TEC of residue 7 and other residues such as I1, Q4, A5, F8, D10, H14, D18, Y21 and L25 as compared to those of ACE2 and SPB25.

The trends of percent helicities in water of $SPB25_{T7L/K11A}$ and $SPB25_{T7L/K11L}$ are relatively similar to SPB25 [23] and slightly higher than that of SBP1 [23]. Our findings suggest that their stabilities in water may be relatively similar to SPB25 and slightly higher than that of SBP1, and the stabilities of these designed SPB25 should be sufficient for their use as peptide binders.

Using the combination of CPD and MD, we designed promising SPB25s with better $\Delta G_{bind\ (MM\text{-}GBSA)}$ to Omicron RBD than human ACE2 receptor and SPB25 by increasing favorable BIs between peptides and the conserved residues of RBD. The results from MD and the MM-GBSA calculation show that the values of $\Delta G_{bind\ (MM\text{-}GBSA)}$ of two best designed peptides ($SPB25_{T7L/K11A}$ and $SPB25_{T7L/K11L}$) are better than those of ACE2 and SPB25. Moreover, their predicted helicities in water are slightly higher than that of SBP1, suggesting that their stabilities are higher than that of SBP1. $SPB25_{T7L/K11A}$ and $SPB25_{T7L/K11L}$ are promising peptide candidates that could possibly be utilized to disrupt BIs between Omicron RBD and ACE2.

Supporting information

S1 Fig. RMSD plots of ACE2, SPB25 and designed peptides in complex with RBD of the omicron variant. The RMSD values of all atoms and backbone atoms are shown in black and grey respectively.
(TIF)

S2 Fig. RMSD plots of SPB25 and designed peptides in water. The RMSD values of all atoms and backbone atoms are shown in black and grey respectively.
(TIF)

S1 Table. The binding free energies of ACE2, SPB25 and all designed peptides to RBD of the omicron variant as calculated by Rosetta and MM-GBSA method.
(PDF)

S2 Table. Hydrogen bond occupations of ACE2, SPB25 and designed peptides binding to RBD of the omicron variant.
(PDF)

Acknowledgments

We would like to thank the Structural and Computational Biology Research Unit, Department of Biochemistry, Faculty of Science, Chulalongkorn University, Thailand for computer resources.

Author Contributions

Conceptualization: Thassanai Sitthiyotha, Surasak Chunsrivirot.

Data curation: Surasak Chunsrivirot.

Formal analysis: Thassanai Sitthiyotha, Wantanee Treewattanawong, Surasak Chunsrivirot.

Funding acquisition: Surasak Chunsrivirot.

Investigation: Thassanai Sitthiyotha, Wantanee Treewattanawong, Surasak Chunsrivirot.

Methodology: Thassanai Sitthiyotha, Surasak Chunsrivirot.

Project administration: Surasak Chunsrivirot.

Resources: Surasak Chunsrivirot.

Supervision: Surasak Chunsrivirot.

Validation: Thassanai Sitthiyotha, Surasak Chunsrivirot.

Visualization: Thassanai Sitthiyotha.

Writing – original draft: Thassanai Sitthiyotha, Surasak Chunsrivirot.

Writing – review & editing: Surasak Chunsrivirot.

References

1. Hui DS, Azhar EI, Madani TA, Ntoumi F, Kock R, Dar O, et al. The continuing 2019-nCoV epidemic threat of novel coronaviruses to global health—The latest 2019 novel coronavirus outbreak in Wuhan, China. International journal of infectious diseases. 2020; 91:264–6. https://doi.org/10.1016/j.ijid.2020.01.009 PMID: 31953166
2. VanBlargan LA, Errico JM, Halfmann PJ, Zost SJ, Crowe JE, Purcell LA, et al. An infectious SARS-CoV-2 B. 1.1. 529 Omicron virus escapes neutralization by therapeutic monoclonal antibodies. Nature medicine. 2022; 28(3):490–5. https://doi.org/10.1038/s41591-021-01678-y PMID: 35046573
3. World Health Organization, Tracking SARS-CoV-2 variants, WHO Official Website. 2022 [cited 2023 28 January]. Available from: https://www.who.int/activities/tracking-SARS-CoV-2-variants/.
4. Oude Munnink BB, Worp N, Nieuwenhuijse DF, Sikkema RS, Haagmans B, Fouchier RA, et al. The next phase of SARS-CoV-2 surveillance: real-time molecular epidemiology. Nature medicine. 2021; 27(9):1518–24. https://doi.org/10.1038/s41591-021-01472-w PMID: 34504335
5. Tai W, He L, Zhang X, Pu J, Voronin D, Jiang S, et al. Characterization of the receptor-binding domain (RBD) of 2019 novel coronavirus: implication for development of RBD protein as a viral attachment inhibitor and vaccine. Cellular & molecular immunology. 2020; 17(6):613–20. https://doi.org/10.1038/s41423-020-0400-4 PMID: 32203189

6. Structure Li F., function, and evolution of coronavirus spike proteins. Annual review of virology. 2016; 3 (1):237.
7. Lu R, Zhao X, Li J, Niu P, Yang B, Wu H, et al. Genomic characterisation and epidemiology of 2019 novel coronavirus: implications for virus origins and receptor binding. The lancet. 2020; 395 (10224):565–74. https://doi.org/10.1016/S0140-6736(20)30251-8 PMID: 32007145
8. Yan R, Zhang Y, Li Y, Xia L, Guo Y, Zhou Q. Structural basis for the recognition of SARS-CoV-2 by full-length human ACE2. Science. 2020; 367(6485):1444–8. https://doi.org/10.1126/science.abb2762 PMID: 32132184
9. Yin W, Xu Y, Xu P, Cao X, Wu C, Gu C, et al. Structures of the Omicron Spike trimer with ACE2 and an anti-Omicron antibody. Science. 2022; 375(6584):1048–53. https://doi.org/10.1126/science.abn8863 PMID: 35133176
10. Huang X, Pearce R, Zhang Y. De novo design of protein peptides to block association of the SARS-CoV-2 spike protein with human ACE2. Aging (Albany NY). 2020; 12(12):11263. https://doi.org/10.18632/aging.103416 PMID: 32544884
11. Lotfi M, Hamblin MR, Rezaei N. COVID-19: Transmission, prevention, and potential therapeutic opportunities. Clinica chimica acta. 2020; 508:254–66. https://doi.org/10.1016/j.cca.2020.05.044 PMID: 32474009
12. Li Z, Yi Y, Luo X, Xiong N, Liu Y, Li S, et al. Development and clinical application of a rapid IgM-IgG combined antibody test for SARS-CoV-2 infection diagnosis. Journal of medical virology. 2020; 92(9):1518–24. https://doi.org/10.1002/jmv.25727 PMID: 32104917
13. Monteil V, Kwon H, Prado P, Hagelkrüys A, Wimmer RA, Stahl M, et al. Inhibition of SARS-CoV-2 infections in engineered human tissues using clinical-grade soluble human ACE2. Cell. 2020; 181(4):905–13. e7. https://doi.org/10.1016/j.cell.2020.04.004 PMID: 32333836
14. Gurwitz D. Angiotensin receptor blockers as tentative SARS-CoV-2 therapeutics. Drug development research. 2020; 81(5):537–40. https://doi.org/10.1002/ddr.21656 PMID: 32129518
15. Cao L, Goreshnik I, Coventry B, Case JB, Miller L, Kozodoy L, et al. De novo design of picomolar SARS-CoV-2 miniprotein inhibitors. Science. 2020; 370(6515):426–31. https://doi.org/10.1126/science.abd9909 PMID: 32907861
16. Wu Y, Wang F, Shen C, Peng W, Li D, Zhao C, et al. A noncompeting pair of human neutralizing antibodies block COVID-19 virus binding to its receptor ACE2. Science. 2020; 368(6496):1274–8. https://doi.org/10.1126/science.abc2241 PMID: 32404477
17. Wójcik P, Berlicki Ł. Peptide-based inhibitors of protein–protein interactions. Bioorganic & medicinal chemistry letters. 2016; 26(3):707–13. https://doi.org/10.1016/j.bmcl.2015.12.084 PMID: 26764190
18. Wang H, Dawber RS, Zhang P, Walko M, Wilson AJ, Wang X. Peptide-based inhibitors of protein–protein interactions: biophysical, structural and cellular consequences of introducing a constraint. Chemical Science. 2021; 12(17):5977–93. https://doi.org/10.1039/d1sc00165e PMID: 33995995
19. Sarma S, Herrera SM, Xiao X, Hudalla GA, Hall CK. Computational design and experimental validation of ACE2-derived peptides as SARS-CoV-2 receptor binding domain inhibitors. The Journal of Physical Chemistry B. 2022; 126(41):8129–39. https://doi.org/10.1021/acs.jpcb.2c03918 PMID: 36219223
20. Zareei S, Pourmand S, Amanlou M. Design of novel disturbing peptides against ACE2 SARS-CoV-2 spike-binding region by computational approaches. Frontiers in Pharmacology. 2022; 13. https://doi.org/10.3389/fphar.2022.996005 PMID: 36438825
21. VK P, Rath SP, Abraham P. Computational designing of a peptide that potentially blocks the entry of SARS-CoV, SARS-CoV-2 and MERS-CoV. PloS one. 2021; 16(5):e0251913. https://doi.org/10.1371/journal.pone.0251913 PMID: 34003827
22. Choudhury AR, Maity A, Chakraborty S, Chakrabarti R. Computational design of stapled peptide inhibitor against SARS-CoV-2 receptor binding domain. Peptide Science. 2022:e24267. https://doi.org/10.1002/pep2.24267 PMID: 35574509
23. Sitthiyotha T, Chunsrivirot S. Computational design of 25-mer peptide binders of SARS-CoV-2. The Journal of Physical Chemistry B. 2020; 124(48):10930–42. https://doi.org/10.1021/acs.jpcb.0c07890 PMID: 33200935
24. Sitthiyotha T, Chunsrivirot S. Computational design of SARS-CoV-2 peptide binders with better predicted binding affinities than human ACE2 receptor. Scientific Reports. 2021; 11(1):1–14.
25. Zhang G, Pomplun S, Loftis AR, Loas A, Pentelute BL. The first-in-class peptide binder to the SARS-CoV-2 spike protein. BioRxiv. 2020; 10(2020.03):19.999318.
26. McCallum M, Czudnochowski N, Rosen LE, Zepeda SK, Bowen JE, Walls AC, et al. Structural basis of SARS-CoV-2 Omicron immune evasion and receptor engagement. Science. 2022; 375(6583):864–8. https://doi.org/10.1126/science.abn8652 PMID: 35076256

27. Gordon JC, Myers JB, Folta T, Shoja V, Heath LS, Onufriev A. H++: a server for estimating p K as and adding missing hydrogens to macromolecules. Nucleic acids research. 2005; 33(suppl_2):W368-W71.

28. Case D, Ben-Shalom I, Brozell S, Cerutti D, Cheatham T, III, Cruzeiro V, et al. AMBER 2018; 2018. University of California, San Francisco. 2018.

29. Leaver-Fay A, Tyka M, Lewis SM, Lange OF, Thompson J, Jacak R, et al. ROSETTA3: an object-oriented software suite for the simulation and design of macromolecules. Methods in enzymology. 487: Elsevier; 2011. p. 545–74. https://doi.org/10.1016/B978-0-12-381270-4.00019-6 PMID: 21187238

30. Du W, Hurdiss DL, Drabek D, Mykytyn AZ, Kaiser FK, González-Hernández M, et al. An ACE2-blocking antibody confers broad neutralization and protection against Omicron and other SARS-CoV-2 variants of concern. Science immunology. 2022:eabp9312. https://doi.org/10.1126/sciimmunol.abp9312 PMID: 35471062

31. Loshbaugh AL, Kortemme T. Comparison of Rosetta flexible-backbone computational protein design methods on binding interactions. Proteins: Structure, Function, and Bioinformatics. 2020; 88(1):206–26. https://doi.org/10.1002/prot.25790 PMID: 31344278

32. Ollikainen N, de Jong RM, Kortemme T. Coupling protein side-chain and backbone flexibility improves the re-design of protein-ligand specificity. PLoS computational biology. 2015; 11(9):e1004335. https://doi.org/10.1371/journal.pcbi.1004335 PMID: 26397464

33. Stranges PB, Kuhlman B. A comparison of successful and failed protein interface designs highlights the challenges of designing buried hydrogen bonds. Protein Science. 2013; 22(1):74–82. https://doi.org/10.1002/pro.2187 PMID: 23139141

34. Sun C, Chen L, Yang J, Luo C, Zhang Y, Li J, et al. SARS-CoV-2 and SARS-CoV spike-RBD structure and receptor binding comparison and potential implications on neutralizing antibody and vaccine development. Biorxiv. 2020.

35. Genheden S, Ryde U. The MM/PBSA and MM/GBSA methods to estimate ligand-binding affinities. Expert opinion on drug discovery. 2015; 10(5):449–61. https://doi.org/10.1517/17460441.2015.1032936 PMID: 25835573

36. Miller BR, III, McGee TD Jr, Swails JM, Homeyer N, Gohlke H, Roitberg AE. MMPBSA. py: an efficient program for end-state free energy calculations. Journal of chemical theory and computation. 2012; 8 (9):3314–21. https://doi.org/10.1021/ct300418h PMID: 26605738

37. Ylilauri M, Pentikäinen OT. MMGBSA as a tool to understand the binding affinities of filamin–peptide interactions. Journal of chemical information and modeling. 2013; 53(10):2626–33. https://doi.org/10.1021/ci4002475 PMID: 23988151

38. Maier JA, Martinez C, Kasavajhala K, Wickstrom L, Hauser KE, Simmerling C. ff14SB: improving the accuracy of protein side chain and backbone parameters from ff99SB. Journal of chemical theory and computation. 2015; 11(8):3696–713. https://doi.org/10.1021/acs.jctc.5b00255 PMID: 26574453

39. Kirschner KN, Yongye AB, Tschampel SM, González-Outeiriño J, Daniels CR, Foley BL, et al. GLYCAM06: a generalizable biomolecular force field. Carbohydrates. Journal of computational chemistry. 2008; 29(4):622–55. https://doi.org/10.1002/jcc.20820 PMID: 17849372

40. Treewattanawong W, Sitthiyotha T, Chunsrivirot S. Computational redesign of Fab CC12. 3 with substantially better predicted binding affinity to SARS-CoV-2 than human ACE2 receptor. Scientific reports. 2021; 11(1):1–15.

41. Salomon-Ferrer R, Gotz AW, Poole D, Le Grand S, Walker RC. Routine microsecond molecular dynamics simulations with AMBER on GPUs. 2. Explicit solvent particle mesh Ewald. Journal of chemical theory and computation. 2013; 9(9):3878–88. https://doi.org/10.1021/ct400314y PMID: 26592383

42. Gotz AW, Williamson MJ, Xu D, Poole D, Le Grand S, Walker RC. Routine microsecond molecular dynamics simulations with AMBER on GPUs. 1. Generalized born. Journal of chemical theory and computation. 2012; 8(5):1542–55.

43. Le Grand S, Götz AW, Walker RC. SPFP: Speed without compromise—A mixed precision model for GPU accelerated molecular dynamics simulations. Computer Physics Communications. 2013; 184 (2):374–80.

44. York DM, Darden TA, Pedersen LG. The effect of long-range electrostatic interactions in simulations of macromolecular crystals: A comparison of the Ewald and truncated list methods. The Journal of chemical physics. 1993; 99(10):8345–8.

45. Hou T, Wang J, Li Y, Wang W. Assessing the performance of the MM/PBSA and MM/GBSA methods. 1. The accuracy of binding free energy calculations based on molecular dynamics simulations. Journal of chemical information and modeling. 2011; 51(1):69–82. https://doi.org/10.1021/ci100275a PMID: 21117705

46. Sun H, Li Y, Shen M, Tian S, Xu L, Pan P, et al. Assessing the performance of MM/PBSA and MM/GBSA methods. 5. Improved docking performance using high solute dielectric constant MM/GBSA and

MM/PBSA rescoring. Physical Chemistry Chemical Physics. 2014; 16(40):22035–45. https://doi.org/10.1039/c4cp03179b PMID: 25205360

47. Sitthiyotha T, Pichyangkura R, Chunsrivirot S. Molecular dynamics provides insight into how N251A and N251Y mutations in the active site of *Bacillus licheniformis* RN-01 levansucrase disrupt production of long-chain levan. PloS one. 2018; 13(10):e0204915.

48. Roe DR, Cheatham TE, III. PTRAJ and CPPTRAJ: software for processing and analysis of molecular dynamics trajectory data. Journal of chemical theory and computation. 2013; 9(7):3084–95. https://doi.org/10.1021/ct400341p PMID: 26583988

49. Nelson DL, Lehninger AL, Cox MM. Lehninger principles of biochemistry: Macmillan; 2008.